Dark sector cosmic fluid interactions as a solution to the observed disagreement in measurements of the Hubble expansion rate

by

Dave Ross Miller

Thesis Submitted in Partial Fulfillment of the
Requirements for the Degree of
Bachelor of Science (Honours)

in the
Department of Physics
Faculty of Science

SIMON FRASER UNIVERSITY
April 24, 2019

Abstract

The standard cosmological model, known as the ΛCDM model, is the simplest model that accurately describes a variety of aspects of the Universe, including the cosmic microwave background (CMB), large scale structure, and accelerated expansion. Independent observational data, including data from the CMB, baryon acoustic oscillations (BAO), and supernovae type Ia (SNe Ia) provide significant statistical support for the ΛCDM model. Despite this support the Hubble expansion rate determined from these observations is inconsistent with direct measurements, presenting a tension of over 4σ. In this examination we attempt to alleviate this tension by looking at an important assumption of the ΛCDM model, the assumption that the energy densities of the different cosmic fluid components evolve independently. To test this we consider pairwise interactions between dark sector cosmic fluid components by introducing terms which allow for energy exchange between components to the right hand side of the Friedmann fluid equations. Making use of Markov Chain Monte Carlo methods we find that energy exchange between cold dark matter (CDM) and dark energy can correct for the discrepancy between CMB measurements of the Hubble expansion rate and direct measurements, but that adding the BAO measurements to the analysis prevents this tension from being fully alleviated. Our findings suggest dark sector cosmic fluid interactions are a strong candidate for physics beyond ΛCDM and warrant additional research.

Keywords: cosmology, Hubble expansion rate, Friedmann equations, cosmic fluid interactions

Acknowledgements

First and foremost, I would like to thank my research supervisor Dr. Levon Pogosian for his willingness to take me on as a student, and for extremely helpful supervision throughout the project. Additionally, I would like to extend my gratitude towards SFU PhD candidate Alex Zucca for his valuable assistance in the early coding stages of the project, and to the entirety of the SFU cosmology group for their positive attitudes and interesting group discussions throughout the last two semesters. I would also like to thank the many teachers over the years whose passion for science encouraged me to pursue a career in physics.

Beyond strictly academic support, I would not have gotten to this point without the support provided by my friends, both at SFU and abroad. To my friends from Salt Lake City and Spearfish, thanks for being there for me all these years through both thick and thin, especially Ryan Terry and Stephen Martinelli, who to this day still tolerate my venting my frustrations while always providing a friendly voice to speak with. To my friends in the Physics Student Association at SFU, I would not have made it to this point in this degree without the supportive community cultivated by your welcoming attitudes. In particular I would like to extend my gratitude towards Symphony-Hsiao Yuan Huang, William Newberry, and Mathew Schneider for being the friendly faces that originally brought me into this group and remained supportive throughout these past few years, and especially to Florian Bär, whose support this past semester, and throughout my undergraduate degree, helped me survive even the toughest of times, I have no doubt I would not have gotten through this semester as successfully without his support.

Finally, I would like to thank my mother Janice, and step-father David here in Vancouver for letting me share their home these last few years and providing unconditional love and support even as academic obligations claimed more and more of my time. To my father Roger in Florida, and my sister Kelly here in Vancouver, I grew up with you two as my support system, you have seen me at my best and at my worst, I would not have made it this far without your encouragement and love. Finally, I can not speak enough for the support my fiancée Lisa has given me throughout these last few years, even as I secluded myself to my office and was unable to spend much time with her she always was supportive, even when it it was exceedingly difficult to be apart for long periods. The results of this dissertation are a testament to the unconditional love and support provided by all of these wonderful people.

Table of Contents

List of Tables

List of Figures

Chapter 1

Introduction

In the past two decades significant observational evidence has led to the ΛCDM model becoming the standard cosmological model [17]. Under the ΛCDM model universal expansion is powered by a cosmological constant vacuum energy (Λ), often referred to as dark energy, with the energy density of matter dominated by cold dark matter (CDM). The Universe is considered to be spatially flat, and obeys the cosmological principle, which says that at the largest scales the Universe should be homogeneous, meaning the same at every point, and isotropic, meaning the same in every direction [27]. Independent sources of observational evidence provides significant statistical support for the ΛCDM model, including evidence from baryon acoustic oscillations (BAO), supernovae type Ia (SNe Ia), and the CMB. Despite this support, model independent direct measurements of the Hubble expansion rate taken by Riess et al. find a Hubble expansion rate that is 4.4σ away from measurements taken from CMB and BAO data, outside the plausible range of reasonable agreement [24]. Due to the model dependent nature of the measurements found from early universe datasets this tension suggests physics beyond ΛCDM.

In this examination we attempt to correct for this tension by looking at an important assumption of the ΛCDM model, the assumption that the energy densities of the different components that make up the matter content of the Universe evolve independently. To examine this we introduce interaction terms that allow for energy exchange between components to the Friedmann fluid equations. Using Markov Chain Monte Carlo (MCMC) methods we test the agreement of these introduced interaction terms with observational data. From this examination we look to shed light on the potential for dark sector interactions as a viable correct to the ΛCDM model.

Chapter 2

Background, Theory, and Motivation

2.1 Big Bang Cosmology

Cosmology attempts to understand the Universe on the grandest of scales. How did the Universe come to be? How does it evolve over time? With nearly 14 billion years of evolution and a nearly unfathomable extent answering these questions is no simple task. It was not until the early 20^{th} century that our modern understanding of the Universe and its evolution started to take form. In 1927, twelve years after Einstein first published his theory of general relativity, Georges Lemaître theorized that if we trace back the evolution of the observable universe that it can mathematically shrink to a single point, and thus, the Big Bang theory was born. Throughout the decades more and more support came in for this once outlandish theory, to the point where it has been accepted as the prevailing cosmological model for our Universe.

Big Bang cosmology is built upon the framework of two primary ideas; general relativity, and the cosmological principle. The cosmological principle says that, when viewed at an appropriately large scale, the Universe should be both homogeneous and isotropic [27]. Without the cosmological principle we would be unable to say that we are not in a special place in the Universe, and if we are in a special place we cannot hope to develop a theory that consistently describes the evolution of the Universe throughout. Invoking this principle allows us to use general relativity to describe the gravitational effects of matter clustering, which we can use to build up an understanding of the evolution of our Universe.

2.2 General Relativity

Quantifying distances between astrophysical objects is not a simple task as evaluation depends on the coordinate system used, observers calculating distances in two different coordinate systems may not agree on the distance to a given object. To determine the true physical distance we must convert coordinate dependent measurements into those indepen-

dent of coordinate system. We do this by making use of a metric, which is a mathematical construct that converts coordinate dependent distances into invariants, the metric is the fundamental object in general relativity [7]. To describe the geometry of spacetime we invoke four-dimensional spacetime metrics, described by

$$ds^2 = g_{\mu\nu} dx^\mu dx^\nu, \tag{2.1}$$

relating the yet to be specified metric tensor, $g_{\mu\nu}$, to the coordinate invariant proper time, ds, where the indices μ and ν go from 0 to 3, with the timelike component corresponding to $dx^0 = dt$ and the remaining indices for the three spatial components [10].

Consider the propagation of free particles through spacetime, as the particles propagate they travel along paths called geodesics, which are paths that minimize the distance between two points [7]. In the simplest flat spacetime, known as Minkowski space, these geodesics are simply straight lines, but we want to determine their paths in a general spacetime. By considering the path of a test particle in a general spacetime and parameterizing each point on the curve it follows by λ, we can use the Euler-Legrange equation to minimize the path, leading to the geodesic equation

$$\frac{d^2 x^\mu}{d\lambda^2} + \Gamma^\mu_{\beta\alpha} \frac{dx^\alpha}{d\lambda} \frac{dx^\beta}{d\lambda} = 0, \tag{2.2}$$

where we define the Christoffel symbol as

$$\Gamma^\mu_{\beta\alpha} \equiv \frac{g_{\mu\nu}}{2} (\partial_\alpha g_{\beta\nu} + \partial_\beta g_{\alpha\nu} - \partial_\nu g_{\alpha\beta}), \tag{2.3}$$

where once again each of the indices goes from 0 to 3 [10].

The preceding steps required no knowledge of the gravitational theory of the geometry of spacetime, best understood through the theory of general relativity. To describe the evolution of the Universe, we want to find a relationship between the curvature of spacetime and the energy density of its components. The metric tensor, $g_{\mu\nu}$, contains information about the curvature of spacetime, but how are we to access this information? It can be shown[1] that the information about curvature can be found from the Ricci tensor, which is defined as

$$R_{\mu\nu} \equiv \partial_\alpha \Gamma^\alpha_{\mu\nu} - \partial_\nu \Gamma^\alpha_{\mu\alpha} + \Gamma^\alpha_{\alpha\beta} \Gamma^\beta_{\mu\nu} - \Gamma^\beta_{\mu\alpha} \Gamma^\alpha_{\nu\beta}, \tag{2.4}$$

taking the trace of this leads to the Ricci scalar

$$R = g^{\mu\nu} R_{\mu\nu} \tag{2.5}$$

[1] See Carroll chapter 4 [7].

[10]. Combining the Ricci tensor, Ricci scalar, and metric tensor leads to the important Einstein tensor, defined as

$$G_{\mu\nu} \equiv R_{\mu\nu} - \frac{1}{2} R g_{\mu\nu}, \tag{2.6}$$

giving a measure of curvature [10].

Einstein was able to relate this measure of curvature to the energy density by using the energy-momentum tensor, $T_{\mu\nu}$, leading to the famous Einstein equation

$$G_{\mu\nu} = 8\pi G T_{\mu\nu}, \tag{2.7}$$

where G is Newton's constant [7]. Without considering perturbations, for a perfect isotropic fluid the energy-momentum tensor is given by

$$T_{\mu\nu} = \begin{pmatrix} -\rho & 0 & 0 & 0 \\ 0 & P & 0 & 0 \\ 0 & 0 & P & 0 \\ 0 & 0 & 0 & P \end{pmatrix}, \tag{2.8}$$

where ρ and P are the energy density and pressure of the fluid, respectively [10]. If we considered perturbations the off-diagonal terms in $T_{\mu\nu}$ would be non-zero, for reasons that will be discussed later we have chosen not to include perturbations in this examination. We nearly have all the tools necessary to develop the equations that describe an expanding universe, we just have to specify the form of $g_{\mu\nu}$.

2.3 The ΛCDM Model

To develop the form of $g_{\mu\nu}$ in an expanding universe it is necessary to first understand the concept of comoving distance. As the Universe expands so does the space between objects, if we imagine a grid of points we want to be able to describe positions on the grid in a way such that the distance between objects on the grid remains constant as the Universe expands. To do so we introduce a scale factor, which we call a, which for simplicity is set to one at the current time; looking back in the past the Universe was smaller, so too was the scale factor. Using this scale factor we are able to define a comoving distance measure which maintains constant distance between objects as the Universe expands. Using this formulation, and invoking natural units[2], in a time dt light travels a comoving distance $d\chi = dt/a$, by integrating over the interval $[t(a), t_o]$ we find that the distance light travels in time dt is

$$\chi(t) = \int_{t(a)}^{t_o} \frac{dt'}{a(t')}, \tag{2.9}$$

[2]Setting the speed of light $c = 1$, we will use this convention throughout.

giving the comoving distance, χ, between an object at $a = 1$ and an object at some scale factor a [10].

We now have the necessary tools to consider the form of the metric tensor, in Minkowski spacetime $g_{\mu\nu}$ takes the form

$$g_{\mu\nu} = \begin{pmatrix} -1 & 0 & 0 & 0 \\ 0 & 1 & 0 & 0 \\ 0 & 0 & 1 & 0 \\ 0 & 0 & 0 & 1 \end{pmatrix}, \tag{2.10}$$

as can be seen by looking at the form of Eq. 2.1 [10]. Using comoving distance we relate this form of the metric to an expanding, but still spatially flat[3], universe. The first component of Eq. 2.10, g_{00}, is a timelike component and is unchanged when considering an expanding universe. As the universe expands, if the current distance to an object is given by x, then in the past the distance was $\chi = a(t)x$, so to generalize Eq. 2.10 for an expanding universe we only have to multiply the remaining diagonal components by $a^2(t)$, leading to the desired form of the metric tensor

$$g_{\mu\nu} = \begin{pmatrix} -1 & 0 & 0 & 0 \\ 0 & a^2(t) & 0 & 0 \\ 0 & 0 & a^2(t) & 0 \\ 0 & 0 & 0 & a^2(t) \end{pmatrix}, \tag{2.11}$$

known as the Friedmann-Robertson-Walker (FRW) metric [10].

Using the FRW metric we are able to find solutions to the Einstein equation (Eq. 2.7), allowing us to relate the evolution of matter in the Universe to the evolution of the scale factor. Using this form we find that the only non-zero components of the Einstein tensor in Eq. 2.6 are

$$G_{00} = 3\left(\frac{\dot{a}}{a}\right)^2, \tag{2.12}$$

and

$$G_{ii} = 2\frac{\ddot{a}}{a} + \left(\frac{\dot{a}}{a}\right)^2, \tag{2.13}$$

where the index $i \neq 0$. Using these expressions along with the form of the energy-momentum tensor, given by Eq. 2.8, in the Einstein equation leads to

$$\left(\frac{\dot{a}}{a}\right)^2 = \frac{8\pi G}{3}\rho, \tag{2.14}$$

[3]Curvature can be introduced here, but our examination focuses on a flat universe, consistent with observations [10].

and

$$\frac{\ddot{a}}{a} = -\frac{4\pi G}{3}(\rho + 3P), \tag{2.15}$$

where ρ and P give the total energy density and pressure of the Universe, these equations are colloquially known as the Friedmann equations[4] [10]. Eq. 2.14 is typically written in terms of the Hubble parameter $H \equiv \dot{a}/a$, giving

$$H^2 = \frac{8\pi G}{3}\rho. \tag{2.16}$$

From these two Friedmann equations we can derive a third Friedmann equation for the evolution of energy density. Noting that the energy density of the Universe must be conserved, this leads us to the ΛCDM continuity equation

$$\dot{\rho}_i + 3H(\rho_i + P_i) = 0, \tag{2.17}$$

where ρ and P are the energy density and pressure of each component of the matter makeup of the Universe [10]. Throughout the rest of this work we will refer to this equation, and its alternate forms, as fluid equations.

To specify the matter content of the Universe we classify components by looking at how their energy density and pressure relate by defining an equation of state (EoS) $P_i = w_i\rho_i$, for some constant w. Replacing P_i in Eq. 2.17 and integrating leads to solutions that scale as $\rho \propto a^{-3(1+w)}$. For all forms of matter where $\rho >> P$, we set $P \simeq 0$, giving a constant $w = 0$, and an energy density that scales as $\rho \propto a^{-3}$, this applies for any non-relativistic gas where the mass dominates the energy density [10]. We will refer to all types of matter with this EoS as simply *matter*[5], we further separate matter into two different components that have the same EoS; baryonic matter, which refers to all matter that interacts with electromagnetic radiation, and cold dark matter (CDM), a poorly understood invisible form of matter that is thought to make up approximately 85% of all matter[27][6]. We use the term *radiation* to refer to any form of matter with an EoS $P = \rho/3$, giving an energy density that scales as $\rho \propto a^{-4}$, this applies for any relativistic gas particles where the kinetic energy term dominates the energy density [10]. In the past few decades observational evidence make it clear that radiation and matter are not enough to describe the matter content of the Universe, instead the current energy makeup seems to be dominated by a mysterious form of vacuum energy with an EoS $P = -\rho$, accounting for approximately 75% of the Universe's

[4]We will differentiate between these equations by referring to Eq. 2.15 as the Friedmann acceleration equation.

[5]Though seemingly confusing, referring to all of the content of the Universe as matter, and separately referring to the pressureless components as *matter* is the standard in cosmology.

[6]The *cold* in cold dark matter refers to the non-relativistic nature of the component.

current energy budget [1]. Though very poorly understood its presence is necessary to explain the accelerated expansion of the Universe [22, 25]. As this EoS leads to an energy density scaling of $\rho \propto a^0$ this is referred to as a cosmological constant vacuum energy, represented by Λ, more commonly refereed to as *dark energy*.

Bringing together these components leads to a set of four independently evolving fluid equations

$$\dot{\rho}_b + 3H\rho_b = 0, \tag{2.18}$$

$$\dot{\rho}_c + 3H\rho_c = 0, \tag{2.19}$$

$$\dot{\rho}_r + 4H\rho_r = 0, \tag{2.20}$$

and

$$\dot{\rho}_\Lambda = 0, \tag{2.21}$$

where the indices b, c, r, and Λ represent baryonic matter, CDM, radiation, and dark energy, respectively. For convenience we introduce the dimensionless density parameter $\Omega_i = \rho_i/\rho_c$, where ρ_c is the critical density, which is the total density required for a flat universe at $a = 1$, given by

$$\rho_c = \frac{3H_\mathrm{o}^2}{8\pi G}, \tag{2.22}$$

where H_o is the value of the Hubble parameter at $a = 1$, giving the current value of the Hubble expansion rate. Using these density parameters introduces a normalization factor to satisfy the critical density, we find that we must have

$$\Omega_{b\mathrm{o}} + \Omega_{c\mathrm{o}} + \Omega_{r\mathrm{o}} + \Omega_{\Lambda\mathrm{o}} = 1, \tag{2.23}$$

where the o indicates the values of the density parameters at $a = 1$. In cosmology it is typically easier to work with the scale factor instead of time as the independent variable, using the chain rule on the derivative term in the fluid equations, recalling that $H = \dot{a}/a$, and re-expressing our fluid equations in terms of the density parameters leads to

$$\Omega_b^{'} + 3\frac{\Omega_b}{a} = 0, \tag{2.24}$$

$$\Omega_c^{'} + 3\frac{\Omega_c}{a} = 0, \tag{2.25}$$

$$\Omega_r^{'} + 4\frac{\Omega_r}{a} = 0, \tag{2.26}$$

$$\Omega_\Lambda^{'} = 0, \tag{2.27}$$

where the $'$ indicates differentiation with respect to a. These equations form a set of four independently evolving differential equations, that are coupled by the algebraic Friedmann

equation (Eq. 2.16), which when rewritten in terms of Ω takes the form

$$H^2 = H_o^2 \left(\frac{\Omega_{bo}}{a^3} + \frac{\Omega_{co}}{a^3} + \frac{\Omega_{ro}}{a^4} + \Omega_{\Lambda o} \right). \tag{2.28}$$

This set of differential equations gives us all we need to determine the evolution of the energy density of the Universe, we only have to specify the initial conditions.

2.4 Support for ΛCDM as the Standard Cosmological Model

In the late 20$^{\text{th}}$ century the discovery of the accelerating expansion of the Universe from observations of supernovae type Ia (SNe Ia) provided the fuel for the ΛCDM model to become the standard cosmological model [22, 25]. In the decades that followed significant observational evidence came in to support this model, but in recent years tensions have arose leading to questions about the completeness of ΛCDM. To consider the support and tensions in the model we will first look at how distances are measured in cosmology.

2.4.1 Distance Measures in Cosmology

Measuring distances to distant astrophysical objects is not so simple, as, due to the travel time of light, when we view distance objects we are not seeing them now, we are seeing them in the past. Recalling the concept of comoving distance introduced in Eq. 2.9, its convenient to re-express this into an integral over a, giving

$$\chi(a) = \int_a^1 \frac{da'}{a^{2'} H(a')}, \tag{2.29}$$

where the additional factor of $1/aH$ appears as a result of changing the integration variable [10]. From here their are two important ways to determine distances in cosmology. the first being the angular diameter distance

$$d_a = \frac{l}{\theta}, \tag{2.30}$$

where l is the known physical extent of the object, and θ is the angle it subtends on the sky[7] [10]. We then relate this expression to the comoving distance $\chi(a)$ by noting that the angle subtended is $\theta = l/a\chi(a)$, allowing us to re-express the angular diameter distance as

$$d_a(a) = a\chi(a). \tag{2.31}$$

From the form of this expression we see that the angular diameter distance is equal to the comoving distance at $a = 1$, but decreases as we look at objects further in the past. Another important distance measure in cosmology is the luminosity distance, which is found

[7]This expression holds for small angles.

by measuring the flux of an object of known luminosity, where the flux is given by

$$F = \frac{L_s}{4\pi x^2}, \tag{2.32}$$

where L_s is the intrinsic luminosity at the source, and x is the distance to the object [10]. We can generalize this expression to an expanding universe by using the comoving distance, leading to the expression

$$F = \frac{L_s a^2}{4\pi \chi(a)^2}, \tag{2.33}$$

allowing us to define the luminosity distance d_l as

$$d_l(a) \equiv \frac{\chi(a)}{a}, \tag{2.34}$$

given an object of known luminosity l, if we measure the flux of the source, we can then determine the luminosity distance [10].

Cosmological measurements to distance objects are typically done by measuring the cosmological redshift (z) of the object. Redshift is the effect where the light from a distance object experiences a wavelength shift to the red side of the visible spectrum, this occurs as a result of an object moving away from us, giving a measure of the recessional velocity of an object with respect to the earth[8] [10]. Mathematically redshift can be found from

$$z = \frac{\lambda_{obs} - \lambda_{emit}}{\lambda_{emit}}, \tag{2.35}$$

where λ_{emit} and λ_{obs} are the wavelengths of the emitted, and observed light, respectively [10]. Redshift is related to the scale factor through the relationship

$$z = \frac{1}{a} - 1, \tag{2.36}$$

allowing us to interchange between the two variables easily [10]. This relationship allows us to repress our distance measures in terms of z, giving

$$\chi(z) = -\int_z^0 \frac{dz'}{H(z')}, \tag{2.37}$$

$$d_a(z) = \frac{\chi(z)}{1+z}, \tag{2.38}$$

and

$$d_l(z) = (1+z)\chi(z). \tag{2.39}$$

[8]Similarly, objects moving towards us have their wavelengths blueshifted.

By measuring the redshift of a distance object for different luminosity and angular diameter distances, we can determine the comoving distance and thus the cosmological parameters in the Hubble parameter. Collectively, comoving distance, luminosity distance, and angular diameter distance give us all we need to determine cosmological distances and to develop support for the ΛCDM model.

2.4.2 Observational Evidence

To measure the flux of an object, and thus determine the luminosity distance, we have to have an object of known luminosity. Astronomers make use of objects known as *standard candles*, which are objects that are known to give out a specific amount of light, one useful standard candle are supernovae type Ia (SNe Ia). SNe Ia are a specific type of supernovae that occur in binary star systems where one of the two is a carbon-oxygen white dwarf [12]. These stars are special in that their rotation rate results in a limiting mass known as the Chandrasekhar mass. When in a binary systems these white dwarfs can accrete mass from their companion star, once they reach the Chandrasekhar mass the star goes supernova [12]. Because these stars are exploding at a known mass, and in a known way, they also have a luminosity that is the same for each of these objects [12].

From luminosity distance measurements of SNe Ia, Riess et al. and Perlmutter et al. were able to find evidence for accelerated expansion [22, 25]. To understand how this is done recall that we have defined the luminosity distance in terms of the comoving distance. Then, recalling the form of the comoving distance as in Eq. 2.37, we see that this has been related to the Hubble expansion rate. Using luminosity distance measurements to determine the comoving distance, and then fitting the curve of comoving distance to a cosmological model allowed them to find $H_{\rm o}$. What they found was that the Universe must have a cosmological constant vacuum energy contributing to the expansion, therefore Ω_Λ must be present, from this evidence of accelerated expansion the ΛCDM model became the standard cosmological model. In the past two decades, since the discovery of cosmic acceleration, additional SNe Ia data provided significant statistical support for the ΛCDM model, and provided significant constraints on the energy density of dark energy [3, 14, 18]. In addition to measurements from SNe Ia, measurements of the cosmic microwave background (CMB) and baryon acoustic oscillations (BAO) furthered the support for the ΛCDM model as the standard cosmological model.

To understand where this additional support comes from its useful to take a step back to the early universe. After the inflationary period of the early universe, the Universe went through a process called reheating, where particles from inflation decayed into a primordial plasma of particles, starting the period of radiation domination [10]. At this stage the primordial plasma was so hot that any baryonic matter that formed was ionized, as the energy of photons exceeded the binding energy of hydrogen such that any electron that tried to bind to the hydrogen nucleus and form a neutral atom was quickly knocked out by these

energetic photons. During this time photons and baryons formed this primordial plasma, overdensities of matter acted to compress the fluid, which in turn brought along with it an increase in the pressure of the photons, pushing them into higher energy levels [11]. The increased radiation pressure acted to oppose this compression effect, as the Universe continued to expand these opposing effects produced lower density regions which were compressed by the surrounding fluid [11]. Collectively the counteracting effects of gravity and the radiation pressure produced oscillations analogous to sound waves. These oscillations propagated through the universe at a remarkable speed of approximately 60% of the speed of light, due to the significant difference between the pressure and density of radiation compared with baryonic matter at this stage of cosmic history [11].

These acoustic density waves continued to propagate throughout the Universe until universal expansion cooled the primordial plasma enough such that the energy of photons fell below the binding energy of hydrogen [21]. At this point electrons were able to bind with ionized hydrogen, forming the first stable neutral hydrogen. This period of the Universe's history is known as recombination, and occurred approximately $375,000$ years after the big bang [21]. Because the baryonic matter is no longer charged, radiation then decoupled from matter and instead began to propagate relatively freely throughout the Universe for the rest of cosmic history [8].

Today the remnants of that radiation are visible as the cosmic microwave background (CMB), thermal black body radiation with a consistent temperature of $\simeq 2.7$ kelvin. Despite this consistent temperature minor anisotropies in the temperature of different parts of the sky have been observed, as we see in Fig. 2.1. The root cause of these anisotropies can be traced back to the aforementioned acoustic density waves, when radiation and matter decoupled the acoustic density waves no longer felt the force of the radiation pressure instead becoming effectively frozen in place [11]. Figure 2.2 shows the intensity of CMB temperature fluctuations as a function of angular size and multipole moments, where the primary peak at $\simeq 1.2^\circ$ gives a sense of the preferred angular scale present in the CMB power spectrum. The angular preference to this peak comes as a direct result of the acoustic density fluctuations on a spherical surface as viewed from our location on Earth [11]. The specific position of the first peak is heavily dependent on the density of matter, while the ratio of the heights of the first and the third peak gives a measure of the value of H_o, allowing us to measure the temperature anisotropies of the CMB and constrain these cosmological parameters [15].

Often referred to as the acoustic length scale, the peak at $\simeq 1.2^\circ$ corresponds to a comoving separation of $\simeq 150$ Mpc [4], the acoustic length scale is related to the angular separation using

$$r_A = (1+z)d_a(z)\Delta\theta, \tag{2.40}$$

[9] `https://www.cosmos.esa.int/web/planck`

[10] `https://map.gsfc.nasa.gov/`

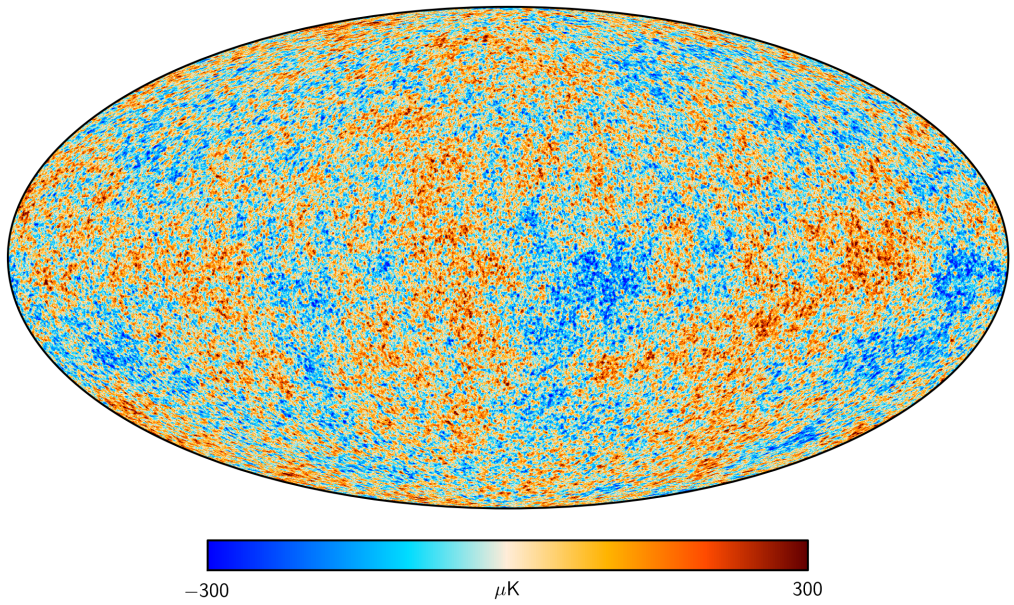

Figure 2.1 Cosmic microwave background radiation map, showing minor fluctuations in temperature of the black body radiation in different parts of the sky. Credit: ESA, Planck satellite, 2015[9].

where d_a is the angular diameter distance at redshift z, as in Eq. 2.38. As a result of this acoustic length scale, in addition to the temperature anisotropies of the CMB the impact of the early universe acoustic density waves can be seen by looking at the large scale distribution of galaxies. At the time of decoupling, when the acoustic density waves were suddenly frozen in place, it left regions of greater density in spherical shells out from where the waves expanded. As dark matter does not interact with electromagnetic radiation, it was not impacted by these acoustic oscillations, resulting in an overdensity region at the center of the spherical shells as well. Figure 2.3 shows an illustration of a series of these rings with radius corresponding to the comoving acoustic length scale, where the spherical shells consist of overdensity regions of baryonic matter, while the dark matter remains clustered at the center of the ring [21]. Over time these denser regions of matter would cluster more and more matter together, forming denser regions of stars and galaxies at both the center and the outside of the spherical shells [11]. Referred to as baryon acoustic oscillations (BAO), this preferred length scale can be used as a *standard ruler*, or an object of known length, enabling us to calculate the angular diameter distance and constrain the value of Ω_b, and as such, look at the evolution of the Hubble expansion rate [8].

[11] `http://www.sdss3.org/surveys/boss.php`

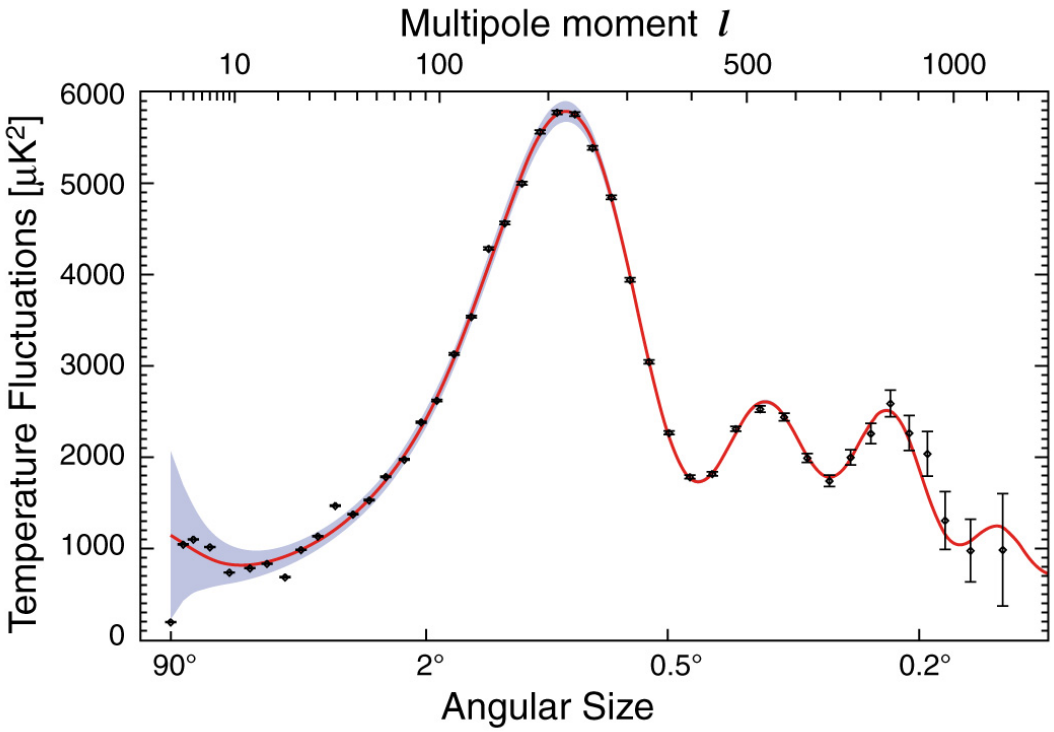

Figure 2.2 Angular power spectrum of CMB temperature fluctuations. Credit: NASA/WMAP Science Team[10].

2.5 Tensions

SNe Ia, CMB temperature anisotropies, and BAO measurements give us a variety of ways to determine the current Hubble expansion rate H_o, but what level of agreement do these different quantities find? In the past decades advancements in technology have enabled research teams to use large sky surveys to vastly improve the quality of data, and to allow for strong estimates of the Hubble expansion rate without extreme uncertainty. In the past three years alone, different calculations of the Hubble expansion rate have found values as follows:

- CMB temperature anisotropy measurements taken by the Planck satellite give an estimate of $(67.66 \pm 0.42)\,\mathrm{km\,s^{-1}\,Mpc}$ [2].
- The first results from the Dark Energy Survery (DES) using both SNe Ia and BAO measurements estimate the value as $(67.77 \pm 1.30)\,\mathrm{km\,s^{-1}\,Mpc}$ [19].
- Measurements from the Baryonic Oscillation Spectroscopic Survery (BOSS) BAO returned a best estimate of $(67.6 \pm 0.7)\,\mathrm{km\,s^{-1}\,Mpc}$ [13].

These different values each agree within uncertainty, providing strong support for the ΛCDM model, however, using precision measurements taken with the Hubble Space Tele-

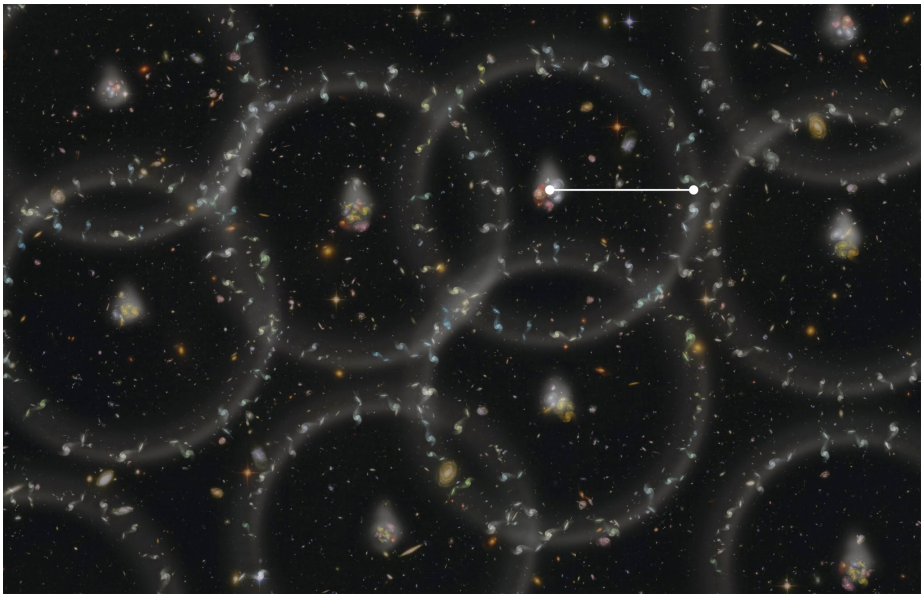

Figure 2.3 Illustration of the distribution of matter from acoustic oscillations. Credit: Z. Rostomian, LBNL[11].

scope (HST), Riess et al. were able to measure the current value of the Hubble expansion rate as $(74.03 \pm 1.42)\,\mathrm{km\,s^{-1}\,Mpc}$ [24]. This measurements of the Hubble expansion rate presents a tension between measurements from the CMB and BAO of around 4.4σ, which for a Gaussian is beyond the plausible level of agreement. A clear tension exists between these different measurements, but why value one over the other? The key to understanding this question is to realize that CMB and BAO measurements are looking at the signature of these early acoustic density waves, as such they are effectively determining the Hubble expansion rate at the point of decoupling, and then using the ΛCDM model to evolve forward and determine the current Hubble expansion rate, meaning these measurements rely on the ΛCDM model accurately describing our Universe. Measurements of the Hubble expansion rate from the HST, however, are direct measurements of the expansion rate, the estimate of $(74.03 \pm 1.42)\,\mathrm{km\,s^{-1}\,Mpc}$ is a model independent determination that knows nothing of ΛCDM.

Could it simply be that the direct HST measurement is suffering from unconsidered uncertainty? To consider this, it is important to understand the concept of the cosmological distance ladder. Angular diameter and luminosity distance measurements require knowing the true length or source luminosity of the object, this is where we rely on the cosmological distance ladder. The cosmological distance ladder is a successive method to determine the distance to distant objects by first looking at closer objects. Using parallax, which is the effect where the apparent position of a star changes relative to other nearby stars as the star moves in the sky, to measure the angular change in the stars position in the sky we can determine the distance to the star [6]. This method only works for stars within around 1

Kpc, which on cosmological scales is not very far at all [6]. We can use this measurement of the distance to a nearby star to determine the stars luminosity, by then using a specific type of star that has the same luminosity in all cases, a standard candle, we can use it to calibrate the distance to further stars of the same type using the determined source luminosity.

A commonly used star type to calibrate cosmological distances is a Cepheid variable, which is a type of rapidly rotating star whose luminosity pulses in a consistent way [6]. By measuring the distance to a nearby Cepheid variables we can use them to calibrate distances to Cepheid variables in more distance galaxies. At large astronomical distances the Cepheid variables luminosity is not bright enough to be measured, in which case we then make use of SNe Ia. By determining the distance to a Cepheid variable in a nearby galaxy that also has SNe Ia data available, we can determine the distance to the SNe Ia, and from this find its source luminosity [6]. SNe Ia explode in a consistent way, so have a consistent luminosity, allowing us to use these objects as standard candles. We can then use the distance determination of this first SNe Ia to calibrate the distances to SNe Ia in much more distant galaxies, as the luminosity of these SNe explosions is strong enough to measure at much larger astronomical distances. The accuracy of these luminosities relies on the initial distance determination to the Cepheid variable, so while there is some uncertainty, the high quality nature of modern data suggests it is not likely to throw off the results too significantly.

Pietrzynski et al. were able to use another type of star, known as an Detached Eclipsing Binary (DEB), a type of binary star system with well defined light curves, to determine the distance to the Large Magellanic Cloud, one of our nearest galactic neighbors, with uncertainty of only 1.3% [23]. From this distance, Riess et al. were able to use the HST to measure the periods of 70 Cepheid variables in the Large Magellanic Cloud to accurately determine their source luminosity [24]. As a check on the distance calculation, they also used independent distance determinations from milky way parallax measurements, and masers in NGC 4258, a source of spectral line emission [24]. The HST has additionally observed Cepheid variables in more distance galaxies that host SNe Ia [26]. Combining their knowledge of Cepheid variable luminosity with HST data from galaxies with both Cepheid variables and SNe Ia they were able to measure the current Hubble expansion rate to the aforementioned value of $(74.03 \pm 1.42)\,\mathrm{km\,s^{-1}}$ Mpc, which takes into account each of the three distance measures to the Large Magellanic Cloud, individual estimates from each distance measure do not cause this value to vary significantly [24]. While some uncertainty exists in this measured expansion rate, it is unlikely to account for the 4.4σ discrepancy between their HST measurements and calculated values from BAO and CMB measurements.

2.6 Physics Beyond ΛCDM

Though the ΛCDM model has been the able to accurately describe many aspects of the Universe, the discrepancy between the model dependant and model independent values of the Hubble expansion rate point to something beyond ΛCDM. Due to our lack of fundamental understanding of dark energy and dark matter, it is reasonable to approach this model with caution. Many possibilities have been theorized to explain this discrepancy, including introducing some curvature, neutrino interactions, a new exotic particle, exotic dark energy with an EoS that is not $w = -1$, amongst others. One particular notable assumption of the ΛCDM model is that it assumes that each of the components energy densities evolve independently of one another, but does this agree with observations? Wang et al. used observational data, including data from BAO, CMB, and SNe Ia to examine the evolution of dark energy density [28]. They found that the data suggests that dark energy density likely changes over time [28], which is at odds with the ΛCDM model, which expects that the energy density of dark energy remains constant throughout cosmic time, as we see from Eq. 2.27.

One possible explanation for this discrepancy is that the assumption that the energy densities of the different components evolve independently is wrong, and that we should consider interactions between various components that result in energy exchange. This possibility is what we want to consider in this research, the question is, how would these potential pairwise interactions impact the mathematical expressions that describe the expansion of the Universe, and how to go about testing potential modifications?

Chapter 3

Examination Methods

3.1 Interactions

We want to develop a method to test pairwise interactions between cosmic fluid components. To do this we introduce interaction terms, which we call Q_{ij}, where i and j are for each component and $i \neq j$, to the right hand side of the individual fluid equations (Eqs. 2.24, 2.25, 2.26, and 2.27). To maintain energy conservation we must have that the right hand side of the sum of the fluid equations remain zero, so if we add Q_{ij} to the right hand side of one of our fluid equations we must have $-Q_{ij}$ in another equation to balance. In principle we could consider pairwise interactions between any of the components, but in this work we have chosen to focus on interactions between the dark sector components, dark energy and CDM. The primary reasons for this are that the radiation density, Ω_r, is dominated by the energy from the CMB, so that by determining the temperature of the CMB we can directly measure Ω_r [20]. The temperature of the CMB has been measured to extreme accuracy, allowing us to simply fix the value of Ω_r in our calculations. Additionally, BAO in the early universe heavily constrain the value of Ω_b, so that we choose not to focus on it either. More specifically, due to the dependence of CMB and BAO measurements on the value of the Hubble expansion rate, the directly determined radiation term is $\Omega_r h^2$, and the constrained baryon term is $\Omega_b h^2$, where in these expressions h is a scaled dimensionless version of H_o, given by

$$H_{\rm o} = 100\, h\, {\rm km\, s^{-1}\, Mpc}, \tag{3.1}$$

throughout the remainder of this work we will typical use the dimensionless h as opposed to the dimensionfull $H_{\rm o}$, but will refer to both interchangeably as the current Hubble expansion rate [10]. In general both radiation and baryonic matter are reasonably well understood, while the dark sector components remain a mystery, so the parameters of these weakly understood dark sector components allow for more wiggle room in a cosmological model. As a result of the focus on dark sector interactions, our modified fluid equations take the form

$$\Omega_b^{'} + 3\frac{\Omega_b}{a} = 0, \tag{3.2}$$

$$\Omega_c^{'} + 3\frac{\Omega_c}{a} = Q, \tag{3.3}$$

$$\Omega_r^{'} + 4\frac{\Omega_r}{a} = 0, \tag{3.4}$$

and

$$\Omega_\Lambda^{'} = -Q, \tag{3.5}$$

where Q is an interaction between CDM and dark energy. As a result of this modification, we now have a coupling between the energy density evolution of CDM and dark energy.

We still need to specify the form of these interaction terms, we chose to focus on three specific forms of interaction terms, one that is proportional to Ω_c, a second that is proportional to Ω_Λ, and finally one that is proportional to both. To do this we introduce an interaction parameter γ, leading to the following set of testable interaction terms

$$Q = Q_{c\Lambda} = \frac{3\gamma_{c\Lambda}\Omega_c}{a}, \tag{3.6}$$

$$Q = Q_{\Lambda c} = \frac{3\gamma_{\Lambda c}\Omega_\Lambda}{a}, \tag{3.7}$$

and

$$Q = Q_{c\Lambda} + Q_{\Lambda c} = \frac{3\gamma_{c\Lambda}\Omega_c}{a} + \frac{3\gamma_{\Lambda c}\Omega_\Lambda}{a}, \tag{3.8}$$

where $c\Lambda$ indicates an interaction between dark sector components that is proportional to Ω_c, and Λc indicates one that is proportional to Ω_Λ. We chose to include the constant 3 in these terms to allow the term that is proportional to CDM to have the same form as the 2nd term on the left hand side of Eq. 3.3, making it a strict proportionality, absorbing this constant into the γ parameter would shift the value of the parameter but would have no impact on the physics. With our interaction terms defined we next implement and test them.

3.2 Implementation

To implement and test these interaction terms we make use of Markov Chain Monte Carlo (MCMC) methods, which are methods to sample N-dimensional parameter space by varying parameters over a large number of iterations, building up a probability distribution over a large number of samples. What follows is a guide to the process used to test the validity of these interaction terms.

- We start by expression our model as a system of differential equations as given by Eqs. 3.2, 3.3, 3.4, and 3.5, for the desired interaction term Q.
- We then define our parameters, both free and fixed. For our free parameters, we use Ω_{bo}, Ω_{co}, h, and any γ interaction parameters for the desired model. For each of these

parameters we have to define both an initial value and bounds for a range of variation. As the variation in the ranges of Ω_{bo} and Ω_{co} depends heavily on the value of h, we first define its variation range. To account for the large difference between calculated values of H_o from CMB and BAO observations ($\sim 67\,\mathrm{km\,s^{-1}\,Mpc}$), and measured values from HST data ($\sim 74\,\mathrm{km\,s^{-1}\,Mpc}$) we opt to allow h to vary between 0.60 and 0.80, at various stages of this work we experimented with both larger and smaller variation ranges. For larger ranges we found that the code had too much trouble finding agreement with the data, and that this resulted in significantly increased computation time and inconsistent results, while for smaller ranges we found that the code would often converge to a small region of parameter space without properly sampling the full range. For Ω_{co} we want to allow for a large amount of freedom as we are specifically allowing for interactions involving this quantity, so we set the bounds from 0.1500 to 0.4000, giving a variation range of $\sim 30\%$ from the value determined by the final release of Planck data [2]. Similarly to h, we tested both larger and smaller variation ranges before settling on this as it returned the most reasonable results while also considering the necessary computation time. For Ω_{bo}, the quantity $\Omega_{bo}h^2$ is heavily constrained from BAO in the early universe, measurements of the primordial abundance of deuterium constrain this quantity to around $\Omega_{bo}h^2 = 0.0220 \pm 0.0005$ [9], scaling this by our range of h gives us a variation range for Ω_{bo} between 0.0330 and 0.0630. For our interaction parameters, γ, we expect a small energy exchange, so we initially allow these parameters to vary between -1 and 1. After initial tests this range was typically lowered to focus in results, pending the specific model results for the given interaction term. In terms of fixed parameters, we keep $\Omega_{ro}h^2$ fixed, for reasons previously discussed. The final density parameter, Ω_Λ, does not have to be included directly as a parameter as its value can always be determined from the normalization condition given in Eq. 2.23. In terms of initial parameter values for Ω_{bo}, Ω_{co}, and h, due to our desire to sample the entire parameter space between the bounds, the initial value is not overly important. Typically we set this to a value towards the center of the range, but as a test of convergence we also test initial values from other regions of parameter space to verify that the results are generally independent of the initial guess.

- Next, using an ODE solver included in the Python package SciPy [16], we numerically integrate our model of differential equations for a randomly sampled series of scale factors using our initial parameter values as the initial conditions, returning the values of each of the four density parameters for every sampled scale factor.

- From these density parameters values, along with the value of H_o determined from the input parameter h, we calculate the algebraic Friedmann equation. Noting that

the code returns $\Omega(a)$, this reduces the Friedmann equation to the form

$$H^2 = H_o^2[\Omega_r(a) + \Omega_b(a) + \Omega_c(a) + \Omega_\Lambda(a)]. \tag{3.9}$$

- Using the values of a along with the calculated values of H we find the comoving distances, as in Eq. 2.29, and from this find the angular diameter, and luminosity distances, as in Eqs. 2.31, and 2.34.

- The next step is to compare these calculated values to data and to find the probability that that the calculated values describe the data, in the form of a likelihood function, which for a Gaussian distribution takes the form

$$L = \prod_i \frac{1}{\sqrt{2\pi\sigma^2}} e^{-\frac{(y_i - \tilde{y_i})^2}{2\sigma^2}} \propto e^{-\chi^2}, \tag{3.10}$$

  where σ is the standard deviation, y_i are the observed data points, and $\tilde{y_i}$ are the model results. As a result, by finding the maximum of the negative log likelihood we can determine the value of χ^2_{min}. Individual likelihoods from each data set are then combined into a composite likelihood. We make use of 4 different data measures in our examination:

  - BOSS BAO data taken by the Sloan Digital Sky Survey-III (SDSS-III) from mapping of the distribution of quasars and luminous red galaxies[1].
  - SNe Ia data from the UnionSN Cosmology Project[2], as well as data from the mutual collaboration of the SDSS-II and Supernova Legacy Survey (SNLS) [5]. It is necessary to include SNe Ia data from multiple sources to have a distribution of values for a large range of redshifts, as individual surveys typically focus on ranges that are too narrow to build a proper distribution.
  - HST direct measurements of H_o [24].
  - Cosmological parameters calculated from measurements of the CMB temperature anisotropies taken from the Planck satellite[3].

- We then use MCMC methods to vary the initial parameter values and explore parameter space, over a large enough number of samples this allows us to build up a distribution of likelihoods for the full parameter space between the bounds, which by finding the maximum of the negative log likelihood allows us to return the value of χ^2_{min}

[1] `http://www.sdss3.org/surveys/boss.php`

[2] `http://supernova.lbl.gov/union/`

[3] `https://www.cosmos.esa.int/web/planck`

for a given model. To achieve this we make use of a widely used suite of code known as Cosmological MonteCarlo (CosmoMC)[4]. CosmoMC is a suite of code designed for use primarily in Fortran, as we are not including perturbations in our analysis this suite was overly complicated for our needs, so we make use of a Python implementation of this code which only depends on the background equations without consideration for perturbations, referred to as SimpleMC[5]. In early stages of the project we considered whether to include perturbations, but decided they were unnecessary. Including perturbations allows for more data to be included in the analysis, and helps to lower the uncertainty of results, but as we were looking to explore the possibility of interaction terms accounting for the tension in the model dependent and model independent measurements of $H_{\rm o}$, as opposed to trying to statistically constraint the value of $H_{\rm o}$, this decrease in uncertainty was not necessary and we decided against including perturbations in this work. Merging our model with the SimpleMC code package allows us to explore this parameter space and build up the desired probability distribution. The information returned by each iteration of the MCMC code are referred to as chains, and include parameter values, likelihoods, χ^2 calculations, and weights, which give an additional measure of the probability of that specific result explaining the data.

- To ensure that we run our MCMC chains long enough we have to consider convergence of our results, which we do in two ways. First off, after each iteration the code checks the maximum value of the negative log likelihood function, any time an iteration results in a new maximum it returns the adjusted maximum. To verify convergence using this criteria we ensure that the sampling has gone a minimum of 3000 iterations between finding a new maximum before stopping the MCMC chains. As a second verification of convergence we restart the chain using very differential initial conditions, if after enough iterations the code converges to results that are very similar to the results of the earlier chains we consider the result to be convergent. The second test is used to verify that the samples have truly explored all of parameter space, as if their were any bias in the initial parameter values this could result in inconsistent results between chains.

- Finally, to visualize the results of the MCMC chains we make use of an MCMC sample analysis Python package known as GetDist[6]. GetDist is a suite of MCMC analysis tools specifically designed for use with CosmoMC chains, using this package we are able to analyze the results of our MCMC chains. For our analysis we make use of three

[4] `https://cosmologist.info/cosmomc/`

[5] `https://github.com/slosar/april`

[6] `https://github.com/cmbant/getdist`

types of plots, 1D probability distributions, 2D contour plots showing the 1σ and 2σ distribution of pairwise parameters, and finally triangle plots, which combine these two features to compare any number of parameters by making a triangular grid of 2D contour plots between each desired parameter, along with 1D probability distributions which are shown along the top right diagonal.

Chapter 4

Results and Discussion

We now present the results of our MCMC chains for the ΛCDM model without interactions, and our three interaction models (Eqs. 3.6, 3.7, and 3.8). We perform an analysis using four different data combinations for each model; Planck+H_o, Planck+H_o+BBAO, Planck+H_o+SNe, and Planck+H_o+BBAO+SNe. The main results of this statistical analysis are summarized in Table 4.1, including the 1σ error range (68% confidence level) for the primary parameters.

4.1 ΛCDM

We start by preforming an analysis of chain results for the ΛCDM model, this model provides a quality check to verify that our MCMC chains are returning results that are reasonable when compared with the estimated values of H_o, while additionally allowing for comparisons to the results of our interaction models. Figure 4.1 shows the triangle plot results for this model, with the most probably values of the parameters along with their 1σ errors included in Table 4.1.

Focusing on the probability distribution for h in the top left of the triangle plot, we see that when we include only the Planck+H_o data sets the chains return a most probably value of $h = 0.691 \pm 0.018$, shifted slightly from the estimated value of H_o given by the Planck collaboration of $(67.66 \pm 0.42)\,\mathrm{km\,s^{-1}\,Mpc}$ [2]. Though the inclusion of the direct measure of H_o from the HST does shift the expected value of the Hubble expansion rate, the value is still more than 3σ away from the measured value. If we include SNe data the distribution becomes narrower, but the shift in peak value is minimal. If we include BBAO data, however, we see the value is shifted much closer to the value determined by the BOSS BAO (BBAO) collaboration of $(67.6 \pm 0.7)\,\mathrm{km\,s^{-1}\,Mpc}$ [13]. Throughout our examination, the BBAO data consistently shifted the results close to the ΛCDM best fit value, this result is not entirely unexpected as the baryonic acoustic oscillation measurements are very sensitive to shifts in the values of the matter density parameters, by including this data, the MCMC chains tended to funnel towards these expected values. Looking closely at Fig. 4.1

Table 4.1. Statistical results of MCMC chains with 68% CL errors.

Model	Data	h	Ω_{co}	$\gamma_{c\Lambda}$	$\gamma_{\Lambda c}$
ΛCDM	Planck+H_o	0.691 ± 0.018	0.234 ± 0.018	...	...
	Planck+H_o+BBAO	0.677 ± 0.008	0.258 ± 0.009	...	...
	Planck+H_o+SNe	0.696 ± 0.013	0.239 ± 0.014	...	...
	Planck+H_o+BBAO+SNe	0.678 ± 0.007	0.257 ± 0.009	...	...
$Q_{c\Lambda}$	Planck+H_o	0.735 ± 0.023	0.217 ± 0.017	0.069 ± 0.032	...
	Planck+H_o+BBAO	0.679 ± 0.007	0.260 ± 0.011	0.013 ± 0.024	...
	Planck+H_o+SNe	0.716 ± 0.019	0.229 ± 0.014	0.046 ± 0.027	...
	Planck+H_o+BBAO+SNe	0.679 ± 0.007	0.258 ± 0.010	0.007 ± 0.021	...
$Q_{\Lambda c}$	Planck+H_o	0.733 ± 0.025	0.218 ± 0.019	...	0.020 ± 0.009
	Planck+H_o+BBAO	0.678 ± 0.008	0.261 ± 0.011	...	0.006 ± 0.009
	Planck+H_o+SNe	0.712 ± 0.018	0.232 ± 0.015	...	0.013 ± 0.081
	Planck+H_o+BBAO+SNe	0.679 ± 0.007	0.257 ± 0.010	...	0.002 ± 0.008
$Q_{c\Lambda} + Q_{\Lambda c}$	Planck+H_o	0.735 ± 0.023	0.217 ± 0.018	0.66 ± 0.20	-0.18 ± 0.06
	Planck+H_o+BBAO	0.677 ± 0.008	0.262 ± 0.011	0.55 ± 0.23	-0.20 ± 0.09
	Planck+H_o+SNe	0.711 ± 0.017	0.233 ± 0.014	0.60 ± 0.22	-0.18 ± 0.07
	Planck+H_o+BBAO+SNe	0.678 ± 0.007	0.260 ± 0.010	0.64 ± 0.21	-0.24 ± 0.08

we can see this trend clearly, the red and green curves in the probability distribution show the results for the two data sets without including BBAO, comparing these to the blue and orange curves we see that the width of the probability distribution is significantly narrower, shifting the peak of the curve to a lower value. We can see the same narrowing effect from the inclusion of the SNe data when comparing the red and green curves, but the effect is much more minor. In all cases the peak of the distribution remains $> 3\sigma$ away from the directly measured value of $(74.03 \pm 1.42)\,\mathrm{km\,s^{-1}\,Mpc}$, which is shown with a dotted grey line, with the yellow band showing the 1σ region for this direct measurement.

In the bottom left of Fig. 4.1 we see the 2D contour plot showing the 1σ (darker shades) and 2σ (lighter) regions. We see that the edge of the 2σ region for only Planck+H_o data falls inside the 1σ region of the direct measurement of H_o, while the rest of the data falls outside the 1σ range. The bottom right plot shows the probability distribution for Ω_{co}, indicating a shift to higher expected CDM density when including BBAO data. Collectively, these results are consistent with our expectations for the ΛCDM model, illustrating the tension between the model dependent and model independent values of H_o. Having found reasonable results for our model without interactions, we can compare and quantify the impact of adding dark sector interactions.

4.2 Interaction terms

We now compare and contrast these results with the results of our MCMC chains with interaction terms. In each of the three interaction model cases we make use of the same four data sets, presenting the statistical results in Table 4.1.

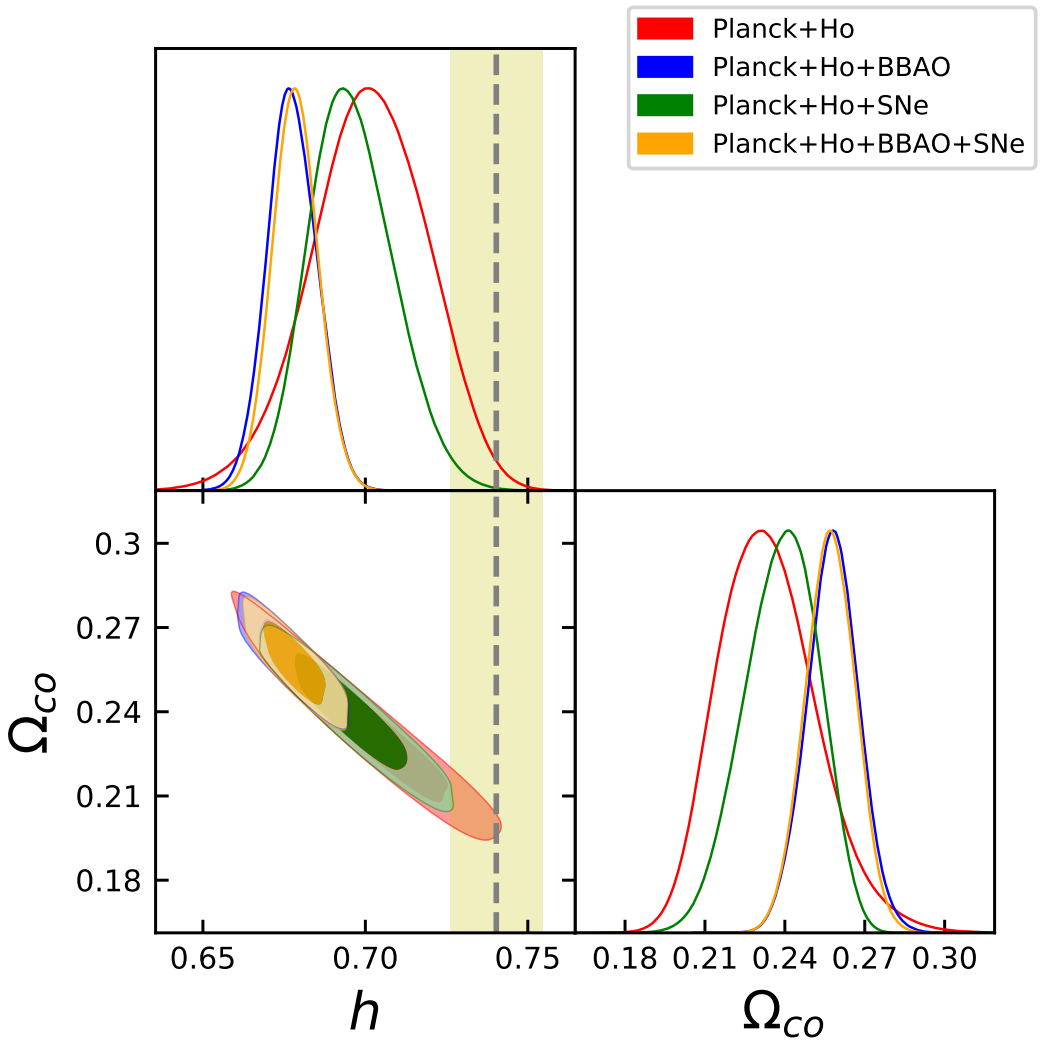

Figure 4.1 Triangle plot for ΛCDM model with four different data combinations showing 1D probability distributions for h and Ω_{co} along the diagonal, with the bottom left showing a 2D contour plot displaying the 1σ and 2σ regions for the given parameters. The yellow band shows the 1σ range for the direct measurement of H_o from Riess et al. [24], with the dashed grey line showing the central value.

4.2.1 $Q_{c\Lambda}$

First considering $Q = Q_{c\Lambda} = (3\gamma_{c\Lambda}\Omega_c)/a$, the results of the chains are shown in Fig. 4.2, noting that we make use of the same type of triangle plot but now also include $\gamma_{c\Lambda}$ in our comparisons. Similarly to the ΛCDM case, when we include BBAO data the peak value of the probability distribution for h converges towards a value near the value determined by the BBAO collaboration of $(67.6 \pm 0.7)\,\mathrm{km\,s^{-1}\,Mpc}$ [13], resulting in a peak value of the probability distribution of the interaction parameter $\gamma_{c\Lambda}$ that fluctuates close to zero. The model dependent nature of these BAO measurements is not conducive to significant changes in the model. If we look at the data sets where BAO is left off, however, we see a significant shift to a higher expected value of h. In particular, when using Planck+H_o data we find a most probable value of $h = 0.735$, which is within the 1σ range of the direct measured value of H_o. This presents a shift of approximately 2σ from the results for this same data set for the ΛCDM model, clearly showing that an interaction of this form can correct for the tension between direct measurements of H_o from the HST and Planck CMB measurements. If we include SNe data, the distribution shifts a bit to a peak value of $h = 0.712$, but the 1σ range of the contour plots for h remains well within the 1σ range of the direct measurement of H_o, and its notably shifted by approximately 1σ from the value returned for this same data set with the ΛCDM model.

Focusing on the probability distribution for $\gamma_{c\Lambda}$ in the center right of Fig. 4.2, we see that in each case the interaction parameter favors a positive value. Recalling that we allowed this parameter to vary between -1 and 1, and nothing the form of the interaction term in Eq. 3.6, we see that the preference for positive $\gamma_{c\Lambda}$ indicates an interaction that leads to energy transfer from CDM into dark energy, shifting the current value of Ω_c down to a lower range of values. In general we find that these results are encouraging and suggest that an interaction between dark sector components that is $\propto \Omega_c$ presents a strong potential correction to the ΛCDM model, but, due to the sensitive model dependence of BAO data this interaction form is unable to alleviate the tension between BAO measurements and direct measurements of the Hubble expansion rate.

4.2.2 $Q_{\Lambda c}$

Next, consider the interaction $Q = Q_{\Lambda c} = (3\gamma_{\Lambda c}\Omega_\Lambda)/a$, where we now have an interaction that is $\propto \Omega_\Lambda$, we present the results of these MCMC chains in Fig. 4.3. We quickly see that the form of the probability distributions and contour plots is extremely similar to the results from the $Q_{c\Lambda}$ interaction. Again when including the BAO data the peak value of the distribution of h converges to a value very close to that of the expected value from the BBAO collaboration, but when we remove this data the results shift to within 1σ of the direct measured value of H_o. Looking at the distribution of $\gamma_{\Lambda c}$ we see that it takes on positive values, again indicating a energy exchange between CDM and dark energy that

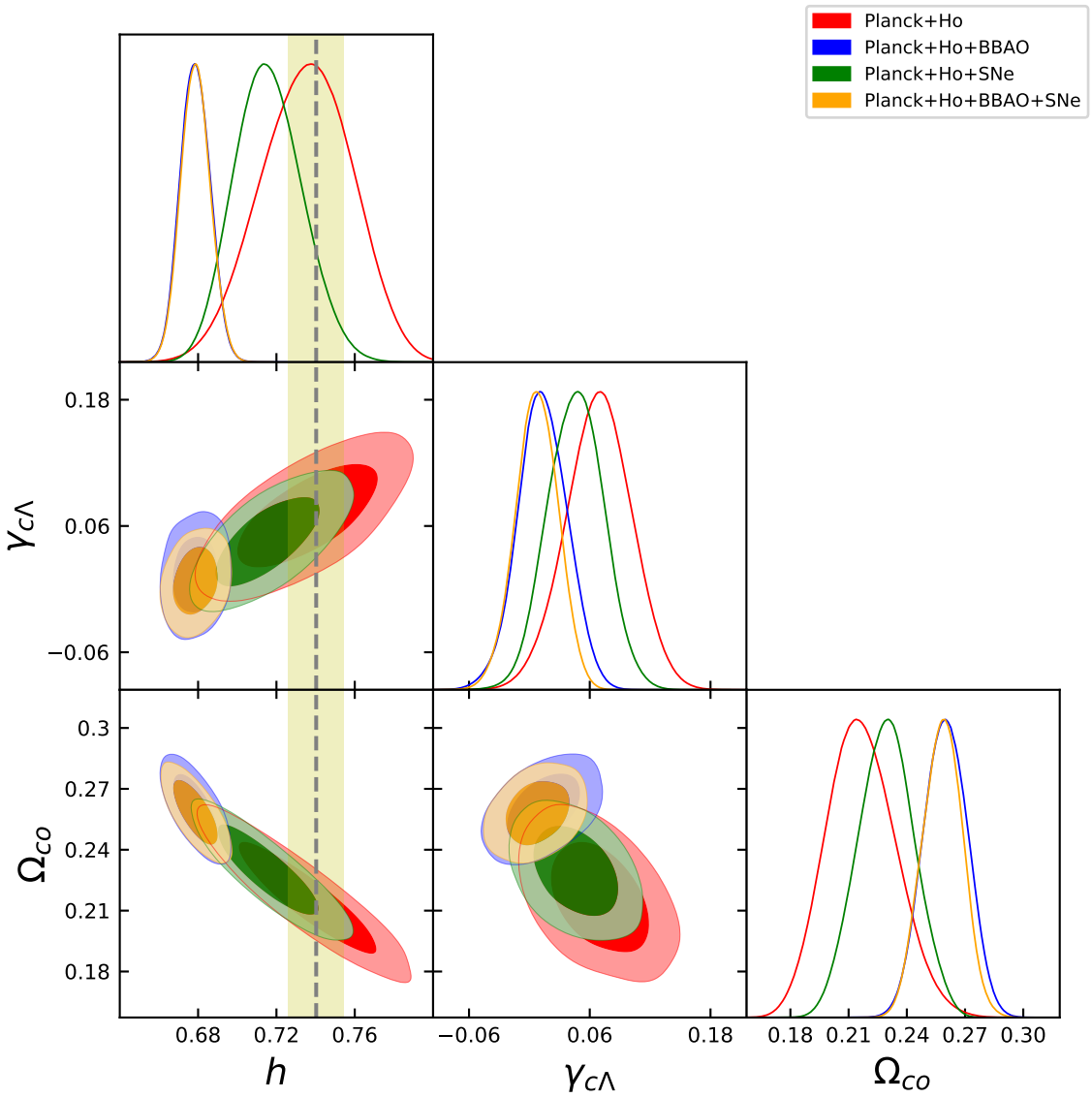

Figure 4.2 Triangle plot as in Fig. 4.1, instead showing results for interaction of form $Q_{c\Lambda}$ (Eq. 3.6).

results in a reduction of the current energy density of CDM when compared to ΛCDM. In general the results for this interaction form are extremely similar to the preceding case and provide additional support for dark sector interactions as a strong candidate to alleviate the tensions between the direct measurements of $H_{\rm o}$ and those from Planck CMB temperature anisotropy measurements.

4.2.3 $Q_{c\Lambda} + Q_{\Lambda c}$

Finally, we look at the interaction form that combines both of these interactions, as given by $Q = Q_{c\Lambda} + Q_{\Lambda c} = (3\gamma_{c\Lambda}\Omega_c + 3\gamma_{\Lambda c}\Omega_\Lambda)/a$, where the results of these chains are given by Fig. 4.4. At first look we see a lot of similarities in these results when compared with the the results for the two individual interaction terms in the preceding sections. The contour plot between Ω_{co} and h presents a very similar form, with chains where BAO was included converging to results similar to ΛCDM, and chains without BAO data shifting to values within 1σ of the direct measured value of $H_{\rm o}$.

Looking at the probability distribution of Ω_{co} we again see a lower range of values when compared to ΛCDM, similar to the results for each of the individual interaction terms. Looking at the distribution of $\gamma_{c\Lambda}$ and $\gamma_{\Lambda c}$ values we see that these distributions have wider peaks than other parameters, this is unsurprising as the nature of these combined interaction terms allows for some degeneracy of solutions, shifting the value of $\gamma_{c\Lambda}$ one way allows for $\gamma_{\Lambda c}$ to shift in the other direction to compensate, and vice versa. We do, however, notice that our results favor the term that is $\propto \Omega_c$ as the stronger interaction, suggesting that energy conversion favors this interaction form. We see that this results in a range of values for $\gamma_{c\Lambda}$ that is notably larger in this two interaction term case as opposed to the case of purely a $Q_{c\Lambda}$ interaction, favoring larger positive values than in the preceding case. This shift has resulted in the value of $\gamma_{\Lambda c}$ typically shifting to negative values, furthering this support for the strength of the $Q_{c\Lambda}$ interaction. Here we importantly have to note that the variation range of γ values was shifted after initial tests. In the case where each interaction parameter was allowed to vary between -1 and 1 we found probability distributions for each γ value that were double peaked Gaussians. In these cases one Gaussian peaked at values similar to what is given in this figure, while the second Gaussian favored lower values of $\gamma_{c\Lambda}$, allowing $\gamma_{\Lambda c}$ to once again take on positive values. In the case of the second Gaussian peak we still found that the $\gamma_{c\Lambda}$ interaction term took on larger values and in general was the dominant interaction term. The height of the two peaks was not similar, with the distribution comparable to Fig. 4.4 presenting a significantly higher peak, leading to our decision to constraint the range further and focus on the range of values associated with the higher peak. Due to the preference for higher values of $\gamma_{c\Lambda}$ we allowed that parameter to have a range that extended beyond 1, though found that solutions rarely took on values above this, as we see from the tail of distribution of $\gamma_{c\Lambda}$ values. Even focusing in the range of each γ value we still have some degeneracy of solutions, which we can see from looking at

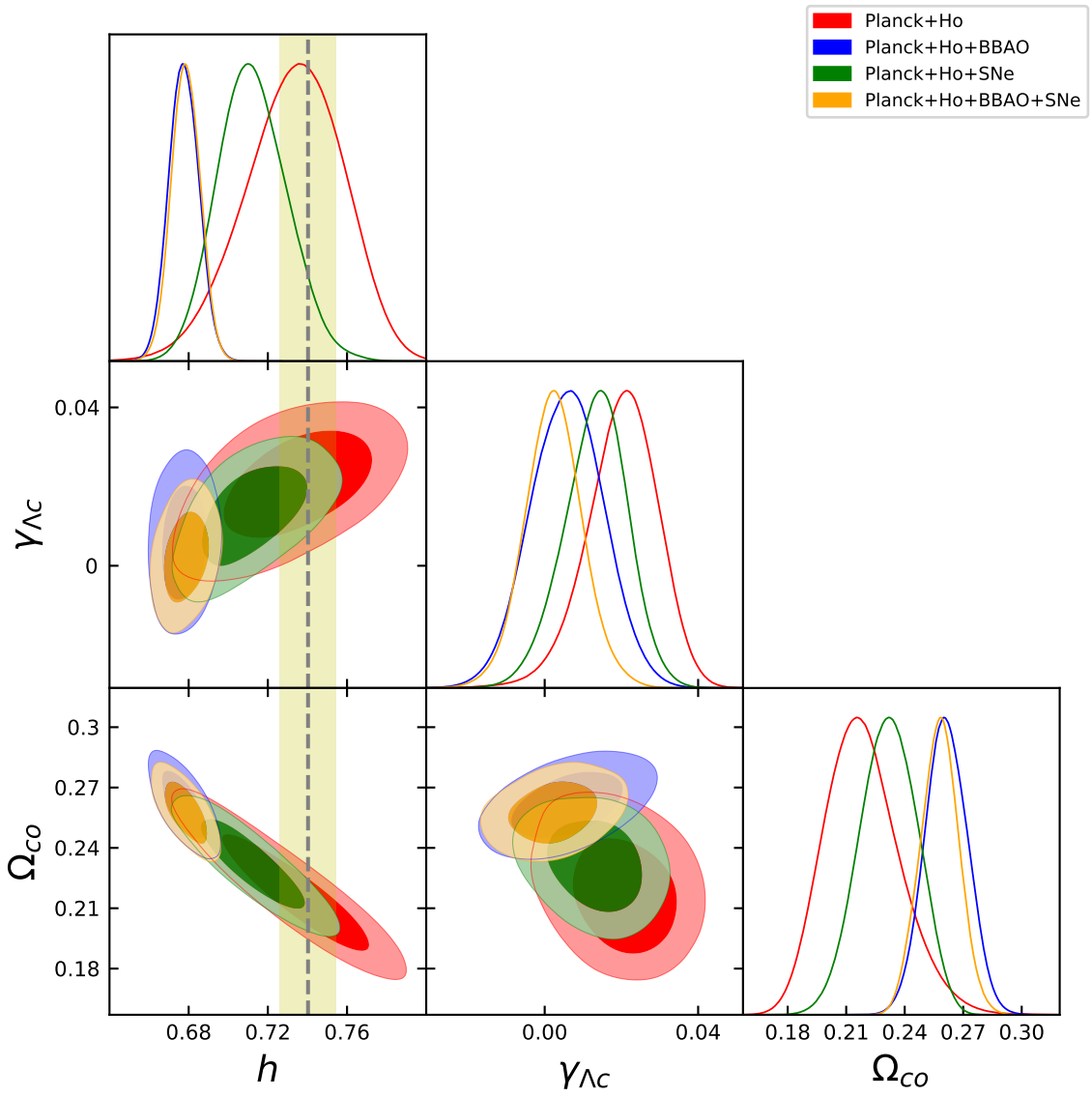

Figure 4.3 Triangle plot as in Fig. 4.1, instead showing results for interaction of form $Q_{\Lambda c}$ (Eq. 3.7).

the blue and orange curves for the probability distributions of the γ parameters. In the case of $\gamma_{c\Lambda}$ the blue curve favors a peak value closer to 0.3, while the orange curve favors one closer to 0.8, whereas when looking at the $\gamma_{\Lambda c}$ distribution we see the opposite trend. In each case, however, the distribution of both h and Ω_{co} is extremely similar, supporting the notion that the degeneracy of solutions of the γ parameters does not impact our primary results. All in all we find that this multiple interaction term returns results similar to our single interaction terms, providing additional support for dark sector interactions as a potential remedy for the tension between direct measurement of the Hubble expansion rate and those from CMB temperature anisotropy measurements, without being able to account for the discrepancy from the parameter sensitive BAO measurements.

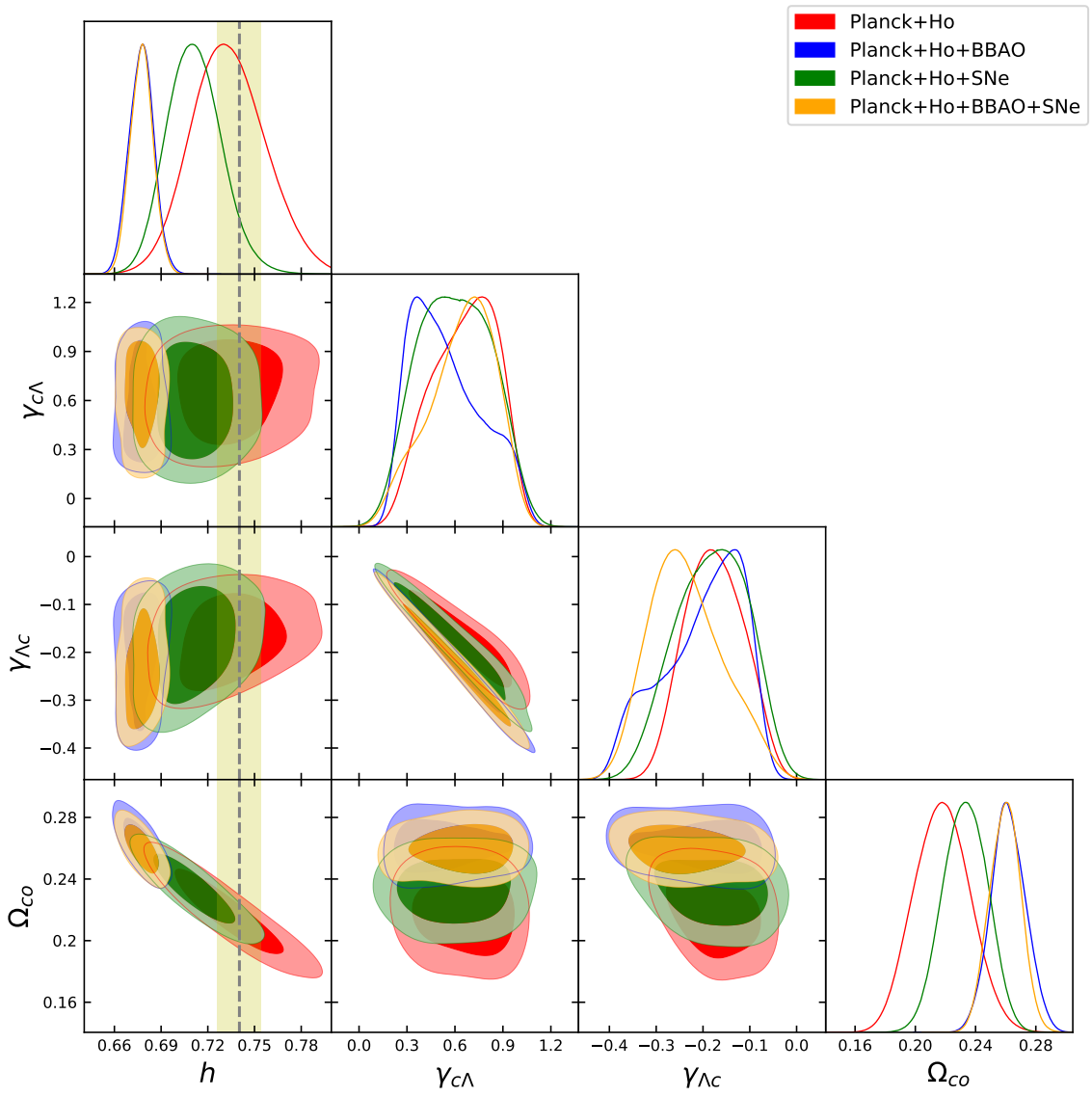

Figure 4.4 Triangle plot as in Fig. 4.1, instead showing results for interaction of form $Q_{c\Lambda} + Q_{\Lambda c}$ (Eq. 3.8).

Chapter 5

Conclusion

Over the past two decades significant observational evidence has come to support the ΛCDM model as the standard cosmological model. Despite this support significant tensions in measurements of the Hubble expansion rate point to physics beyond ΛCDM. In this work we have demonstrated that introducing interactions that allow for energy exchange between dark sector components to the ΛCDM model alleviates the tension between HST measurements of the Hubble expansion rate and those from Planck CMB data. While these tensions were corrected for, the significant sensitivity of BAO measurements to changes in model parameters prevented a full alleviation with all available data. All in all we find that dark sector interactions are a strong candidate as an extension to the ΛCDM model and warrant additional research. Future continuations of this work would include testing more exotic functional forms of these interactions, as well as potentially introducing perturbations.

Bibliography

[1] P. A. R. Ade et al. Planck 2015 results. XIII. Cosmological parameters. *Astron. Astrophys.*, 594:A13, 2016.

[2] N. Aghanim et al. Planck 2018 results. VI. Cosmological parameters. *Submitted to Astron. Astrophys.*, 2018.

[3] P. Astier et al. The Supernova Legacy Survey: measurement of Ω_M, Ω_Λ and w from the first year data set. *Astron. Astrophys.*, 447:31, 2006.

[4] B. A. Bassett and R. Hlozek. *Baryon Acoustic Oscillations in Dark Energy: Observational and Theoretical Approaches.* Cambridge University Press, 2010.

[5] M. Betoule et al. Improved cosmological constraints from a joint analysis of the SDSS-II and SNLS supernova samples. *Astron. Astrophys.*, 568:A22, 2014.

[6] B. W. Carroll and D. A. Ostlie. *An Introduction to Modern Astrophysics.* Addison-Wesley, 2nd edition, 2007.

[7] S. Carroll. *Spacetime and Geometry: An Introduction to General Relativity.* Benjamin Cummings, 2003.

[8] C. Cheng and Q. Huang. An accurate determination of the Hubble constant from Baryon Acoustic Oscillation datasets. *Sci. China Phys. Mech. Astron.*, 58(9):599801, 2015.

[9] R. Cooke, M. Pettini, R. A. Jorgenson, M. T. Murphy, and C. C. Steidel. Precision measures of the primordial abundance of deuterium. *Astrophys. J.*, 781(1):31, 2014.

[10] S. Dodelson. *Modern Cosmology.* Academic Press, Elsevier Science, 2003.

[11] D. J. Eisenstein and C. L. Bennett. Cosmic sound waves rule. *Phys. Today*, 61(4):44, 2008.

[12] A. V. Filippenko. Type Ia supernovae and cosmology. *Astrophys. Space Sci. Libr.*, 332:97, 2005.

[13] J. N. Grieb et al. The clustering of galaxies in the completed SDSS-III Baryon Oscillation Spectroscopic Survey: Cosmological implications of the Fourier space wedges of the final sample. *Mon. Not. Roy. Astron. Soc.*, 467(2):2085, 2017.

[14] M. Hicken et al. Improved Dark Energy Constraints from 100 New CfA Supernova Type Ia Light Curves. *Astrophys. J.*, 700:1097, 2009.

[15] W. Hu and M. J. White. Acoustic signatures in the cosmic microwave background. *Astrophys. J.*, 471:30, 1996.

[16] E. Jones et al. SciPy: Open source scientific tools for Python, 2001–.

[17] A. Joyce, B. Jain, J. Khoury, and M. Trodden. Beyond the cosmological standard model. *Physics Reports*, 568:1, March 2015.

[18] M. Kowalski et al. Improved Cosmological Constraints from New, Old, and Combined Supernova Data Sets. *Astrophys. J.*, 686:749, 2008.

[19] E. Macaulay et al. First Cosmological Results using Type Ia Supernovae from the Dark Energy Survey: Measurement of the Hubble Constant. *Mon. Not. Roy. Astron. Soc.*, 486(2):2184, 2018.

[20] J. C. Mather, D. J. Fixsen, R. A. Shafer, C. Mosier, and D. T. Wilkinson. Calibrator Design for the COBE Far-Infrared Absolute Spectrophotometer (FIRAS). *Astrophys. J.*, 512:511, 1999.

[21] Will J. Percival. Baryon Acoustic Oscillations: A Cosmological Ruler. *Phys. Today*, 70(12):32, 2007.

[22] S. Perlmutter et al. Measurements of Ω and Λ from 42 High-Redshift Supernovae. *Astrophys. J.*, 517:565, 1999.

[23] G. Pietrzynski et al. A distance to the large magellanic cloud that is precise to one per cent. *Nature*, 567:200, 2019.

[24] A. G. Riess, S. Casertano, W. Yuan, L. M. Macri, and D. Scolnic. Large Magellanic Cloud Cepheid Standards Provide a 1% Foundation for the Determination of the Hubble Constant and Stronger Evidence for Physics Beyond ΛCDM. *Accepted by Astrophys. J.*, 2019.

[25] A. G. Riess et al. Observational Evidence from Supernovae for an Accelerating Universe and a Cosmological Constant. *Astrophys. J.*, 116:1009, 1998.

[26] A. Sandage et al. The Hubble Constant: A Summary of the Hubble Space Telescope Program for the Luminosity Calibration of Type Ia Supernovae by Means of Cepheids. *Astrophys. J.*, 653:843, 2006.

[27] R. von Marttens, L. Casarini, D. F. Mota, and W. Zimdahl. Cosmological constraints on parameterized interacting dark energy. *Phys. Dark Univ.*, 23:100248, 2019.

[28] Y. Wang, L. Pogosian, G. Zhao, and A. Zucca. Evolution of dark energy reconstructed from the latest observations. *Astrophys. J. L.*, 869(1):8, 2018.